Modeling the electromagnetic cavity mode contributions to the THz emission from triangular $Bi_2Sr_2CaCu_2O_{8+\delta}$ mesas.

Richard A. Klemm,[1,*] Kaveh Delfanazari,[2,3,4] Manabu Tsujimoto,[2,3,4] Takanari Kashiwagi,[2,3,4] Takeo Kitamura,[2,3,4] Takashi Yamamoto,[2,3,4] Masashi Sawamura,[2,3,4] Kazuya Ishida,[2,3,4] Toshiaki Hattori,[2,3] and Kazuo Kadowaki[2,3,4]

[1]*Department of Physics, University of Central Florida, Orlando, Florida 32816, USA*
[2]*Graduate School of Pure & Applied Sciences, University of Tsukuba, 1-1-1, Tennodai, Tsukuba, Ibaraki 305-8573, Japan*
[3]*CREST, Japan Science and Technology Agency, Kawaguchi Center Building, 4-1-8, Honcho, Kawaguchi, Saitama 332-0012, Japan*
[4]*WPI-MANA, 1-1, Namiki, Tsukuba, Ibaraki 305-0044, Japan*

(Dated: July 31, 2012)

In order to understand the radiation observed from the intrinsic Josephson junctions in triangular $Bi_2Sr_2CaCu_2O_{8+\delta}$ mesas, we calculate the transverse magnetic (TM) electromagnetic modes for thin equilateral cavities. A new set of distinct but degenerate TM modes coexists with the known modes of Helszajn and James, but are expected to lead to distinct radiation angular distribution patterns. Although we have been unable to solve for the exact TM modes of a thin cavity of general acute isosceles triangular shape, we solved exactly the closely related problems of the TM cavity modes of two thin circumscribing "pie-shaped" wedges, which provide highly accurate approximations to very acute isosceles triangular cavities.

PACS numbers:

INTRODUCTION

There has long been a gap in the electromagnetic (EM) spectrum for continuous-wave coherent sources, especially those that can be held in one hand by an ordinary person.[1, 2] This gap could be filled using the Josephson effect in a layered superconductor.[3] Long after the discovery that the high transition temperature T_c superconductor, $Bi_2Sr_2CaCu_2O_{8+\delta}$ (Bi2212), behaves as a stack of intrinsic Josephson junctions (IJJs), [4] application of a dc voltage V across the IJJs led to the emission of intense, coherent, and continuous-wave radiation in the terahertz (THz) frequency regime.[5, 6] In most experiments, the samples were rectangular mesas prepared by either Ar or focussed ion bean (FIB) milling of a small underdoped single crystal of Bi2212.[5–18] In some cases, the mesas had circular or nearly square cross-sections. [11, 13, 16, 18] In all cases, the coherent radiation emitted satisfied the Josephson frequency f relation, $f = 2eV/(Nh)$, where e is the electronic charge, N is the effective number of active junctions, and h is Planck's constant.[5–20] In addition, the insulating nature of the Bi2212 mesas for electric polarization normal to the junctions causes the mesas to behave as EM cavities. The overall radiation has usually been found to be enhanced when f is locked onto a resonant frequency $f^c_{n,m}$ of the transverse magnetic (TM) EM cavity mode appropriate to the particular mesa shape. Although stand-alone mesas prepared by coating the top and bottom of the mesa with Au and placing it on a non-superconducting substrate appear to give rise to large enhancements of the radiation at certain $f^c_{n,m}$ frequencies, FIB milling processes appear to give rise to more complex boundary conditions, leading to a reduced importance of the cavity mode frequencies, as was also found for the radiation emitted from the internal current-voltage characteristic (IVC) branches.[18]

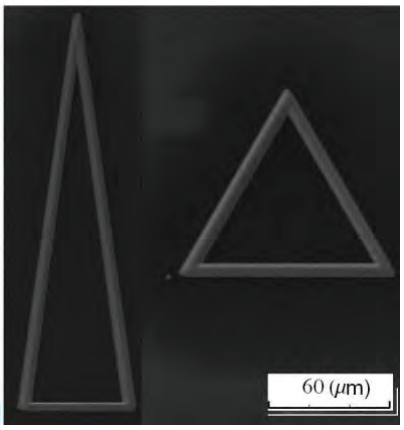

FIG. 1: Scanning ion microscope image of two triangular Bi2212 mesas.[21]

An important feature of the radiation is that under various conditions, it can be made quite tunable.[10, 17, 18] The conditions studied to date are the removal of the precise TM boundary conditions by FIB milling, which creates a mesa by forming a groove about a central region, variation of the bath temperature T and the applied V, and observation of the radiation from the internal IVC branches.[10, 17, 18]

Recently, another method of achieving tunability has

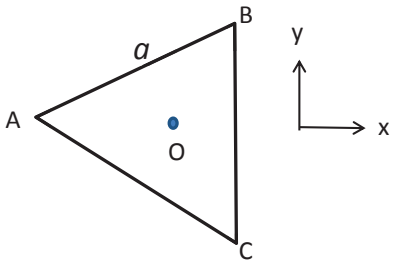

FIG. 2: Sketch of an equilateral triangle of side a, with the center of gravity at the origin O.

been studied.[21] In this method, the thin mesas were chosen to have either equilateral or acute isosceles triangular shapes, as shown in Fig. 1. Although the TM mode frequencies for equilateral triangular mesas (or patch antennas) are well known,[22] the angular distribution of the radiation from such cavities has not been carefully calculated. Here we show that the wave functions originally obtained by Helszajn and James,[22] while correct, comprise only part of the full solution, which also includes a degenerate set of different wave functions.

However, thin acute isosceles triangular cavities are intrinsically more interesting due to their large density of cavity mode states. Unfortunately, an exact solution of the mode frequencies and wave functions for general acute isosceles triangular mesas has not yet been presented. Nevertheless, highly accurate formulas for the frequencies and wave functions for very acute isosceles triangular mesas are easy to obtain, as shown in the following.

EQUILATERAL TRIANGULAR MESAS

A sketch of a thin equilateral triangular mesa of side a is shown in Fig. 2. The origin is taken to be the center of gravity O, and hence the corners are at $A = \left(-\frac{a}{\sqrt{3}}, 0\right)$, $B = \left(\frac{a}{2\sqrt{3}}, \frac{a}{2}\right)$, $C = \left(\frac{a}{2\sqrt{3}}, -\frac{a}{2}\right)$.

Equilateral triangular mesa wave functions

Following Helszajn and James,[22] we take one contribution $\Psi^{e,(1)}_{\ell,m,n}(x,y)$ to the magnetic vector potential $A_z(x,y)$ (*i. e.*, the wave function) to have the form

$$\begin{aligned}\Psi^{e,(1)}_{\ell,m,n}(x,y) &= \cos\Big[\Big(\frac{2\pi x}{\sqrt{3}a}+\frac{2\pi}{3}\Big)\ell\Big]\cos\Big[\frac{2\pi(m-n)y}{3a}\Big]\\ &+\cos\Big[\Big(\frac{2\pi x}{\sqrt{3}a}+\frac{2\pi}{3}\Big)m\Big]\cos\Big[\frac{2\pi(n-\ell)y}{3a}\Big]\\ &+\cos\Big[\Big(\frac{2\pi x}{\sqrt{3}a}+\frac{2\pi}{3}\Big)n\Big]\cos\Big[\frac{2\pi(\ell-m)y}{3a}\Big],\end{aligned} \tag{1}$$

where ℓ, m, and n are integers. This form exhibiting elementary separation of the variables x and y is an even function about the line passing between the origin and the corner at A.

In addition to $\Psi^{e,(1)}_{\ell,m,n}(x,y)$, there is another form exhibiting elementary separation of spatial variables,

$$\begin{aligned}\Psi^{o,(1)}_{\ell,m,n}(x,y) &= \cos\Big[\Big(\frac{2\pi x}{\sqrt{3}a}+\frac{2\pi}{3}\Big)\ell\Big]\sin\Big[\frac{2\pi(m-n)y}{3a}\Big]\\ &+\cos\Big[\Big(\frac{2\pi x}{\sqrt{3}a}+\frac{2\pi}{3}\Big)m\Big]\sin\Big[\frac{2\pi(n-\ell)y}{3a}\Big]\\ &+\cos\Big[\Big(\frac{2\pi x}{\sqrt{3}a}+\frac{2\pi}{3}\Big)n\Big]\sin\Big[\frac{2\pi(\ell-m)y}{3a}\Big],\end{aligned} \tag{2}$$

which is odd about $\overline{OA}$, but was not discussed by Helszajn and James.[22] We note that the second and third terms in Eqs. (1) and (2) are obtained from the first terms by counterclockwise cyclic permutations of the indices: $(\ell, m, n) \to (m, n, \ell) \to (n, \ell, m)$.

We first note that requiring $\Psi^{e,(1)}_{\ell,m,n}$ and $\Psi^{o,(1)}_{\ell,m,n}$ to satisfy the wave equation leads to

$$k^2_{\ell,m,n} = \Big(\frac{2\pi}{3a}\Big)^2[(m-n)^2+3\ell^2] \tag{3}$$

$$= \Big(\frac{2\pi}{3a}\Big)^2[(n-\ell)^2+3m^2] \tag{4}$$

$$= \Big(\frac{2\pi}{3a}\Big)^2[(\ell-m)^2+3n^2]. \tag{5}$$

Setting $\ell = -n - m$ satisfies all three of these equations for both $\Psi^{e,(1)}_{\ell,m,n}$ and $\Psi^{o,(1)}_{\ell,m,n}$, leading to

$$k_{m,n} = \frac{4\pi}{3a}\sqrt{n^2+mn+m^2}. \tag{6}$$

Next, we note that symmetry allows for two additional even and two additional odd degenerate wave function forms obtained by $\pm 120^\circ$ rotations of the axes about the origin, which wave functions may be written as

$$\Psi^{e,(2,3)}_{\ell,m,n}(x,y) = \Psi^{e,(1)}_{\ell,m,n}\Big(-\frac{x}{2}\pm\frac{y\sqrt{3}}{2}, -\frac{y}{2}\mp\frac{x\sqrt{3}}{2}\Big), \tag{7}$$

$$\Psi^{o,(2,3)}_{\ell,m,n}(x,y) = \Psi^{o,(1)}_{\ell,m,n}\Big(-\frac{x}{2}\pm\frac{y\sqrt{3}}{2}, -\frac{y}{2}\mp\frac{x\sqrt{3}}{2}\Big), \tag{8}$$

respectively, where again $\ell + m + n = 0$. These wave functions are respectively even and odd functions about the lines passing through the origin and the corners at B and C in Fig. 2, respectively. Hence, a full description of the modes requires inclusion of the six degenerate wave functions for each mode indexed by (n, m),

$$A_z(x,y) = \sum_{n,m}\sum_{i=1}^{3}\sum_{\alpha=e,o} C^{\alpha,(i)}_{n,m}\Psi^{\alpha,(i)}_{-n-m,m,n}(x,y), \tag{9}$$

where the $C^{\alpha,(i)}_{n,m}$ are constants. To the extent that the cavity is invariant under 120° rotations, the odd $C^{o,(i)}_{n,m}$ are

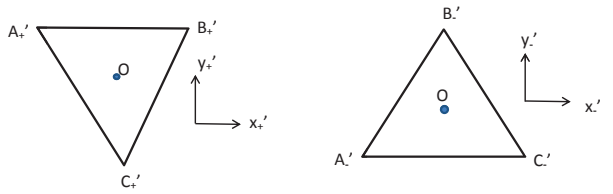

FIG. 3: Sketches of the equilateral triangle in Fig. 2 rotated about the origin by 30° clockwise (left) and counterclockwise (right), with the new respective coordinates $(x'_\pm, y'_\pm)$, and the positions of the corners in the rotated configurations are labeled $A'_\pm$, $B'_\pm$, and $C'_\pm$, respectively.

all equivalent for $i = 1, 2, 3$, as are the even $C^{e,(i)}_{n,m}$, but the odd and even constants are generally independent, and must be treated as arbitrary parameters. Local hot spots or some other imperfections could break this rotational symmetry, giving rise to six distinct $C^{\alpha,(i)}_{n,m}$.[8, 10, 11]

Equation (9) of course assumes that both the even and odd functions satisfy the TM boundary conditions. Since $\Psi^{\alpha,(2,3)}_{\ell,m,n}(x, y)$ are merely rotations by $\pm 120°$ about the origin of $\Psi^{\alpha,(1)}_{\ell,m,n}(x, y)$, it suffices to study $\Psi^{\alpha,(1)}_{\ell,m,n}(x, y)$ for $\alpha = e, o$.

TM boundary conditions

For the TM modes, the component of the magnetic field parallel to the boundaries must vanish on the boundaries. From the Maxwell equations $\boldsymbol{B} = \boldsymbol{\nabla} \times \boldsymbol{A}$ and $\boldsymbol{E} = -\frac{\partial \boldsymbol{A}}{\partial t}$, on the right boundary ($\overline{BC}$) parallel to the y axis in Fig. 2, H_y is proportional to $\frac{\partial E}{\partial x}$. The TM^z modes for the odd wave function $\Psi^{o,(1)}_{\ell,m,n}(x, y)$ must then satisfy

$$\frac{\partial \Psi^{o,(1)}_{\ell,m,n}(x, y)}{\partial x}\Big|_{x=a/(2\sqrt{3})} = 0, \tag{10}$$

$$0 = -\frac{2\pi}{\sqrt{3}a}\Big(\ell \sin(\pi\ell)\sin\Big[\frac{2\pi(m-n)y}{3a}\Big] + (\ell, m, n) \to (m, n, \ell) + (\ell, m, n) \to (n, \ell, m)\Big), \tag{11}$$

which is trivially satisfied for arbitrary y, since $\sin(\pi\ell) = \sin(\pi m) = \sin(\pi n) = 0$ for integral (ℓ, m, n). A similar requirement for $\Psi^{e,(1)}_{\ell,m,n}(x, y)$ is obtained by replacing $\sin[2\pi(m-n)y/(3a)]$ with $\cos[2\pi(m-n)y/(3a)]$ in Eq. (11).

To test whether $\Psi^{\alpha,(1)}_{\ell,m,n}(x, y)$ satisfies the TM boundary conditions on the $\overline{AB}$ and $\overline{AC}$ sides, it is useful to rotate the equilateral triangle by 30° clockwise (+) and counterclockwise (-) about the origin, as indicated in Fig. 3. In these two cases, the coordinate systems may be written in terms of (x, y) as

$$x = x'_\pm\sqrt{3}/2 \mp y'_\pm/2, \tag{12}$$
$$y = y'_\pm\sqrt{3}/2 \pm x'_\pm/2. \tag{13}$$

In order to satisfy the TM boundary conditions on the $\overline{AB}$ and $\overline{AC}$ sides, we therefore require

$$\frac{\partial \Psi^{\alpha,(1)}_{\ell,m,n}(x'_\pm, y'_\pm)}{\partial y'_\pm}\Big|_{y'_\pm = \pm a/(2\sqrt{3})} = 0 \tag{14}$$

for $\alpha = e, o$. It is then straightforward to obtain for $\alpha = o$ that

$$\begin{aligned} 0 = \ell\Big(&\sin(\pi\ell\tilde{x}_\pm)\sin[\pi\tilde{x}_\pm(m-n)/3] \\ &- \cos(\pi\tilde{x}_\pm m)\cos[\pi\tilde{x}_\pm(n-\ell)/3] \\ &+ \cos(\pi\tilde{x}_\pm n)\cos[\pi\tilde{x}_\pm(\ell-m)/3]\Big) \\ &+(\ell, m, n) \to (m, n, \ell) \\ &+(\ell, m, n) \to (n, \ell, m), \end{aligned} \tag{15}$$

where

$$\tilde{x}_\pm = x'_\pm/a + 1/2. \tag{16}$$

Using $\sin(a)\sin(b) = [\cos(a-b) - \cos(a+b)]/2$, $\cos(a)\cos(b) = [\cos(a+b) + \cos(a-b)]/2$, and setting $\ell = -m - n$ in order to satisfy the wave equation, the term proportional to $\ell = -m - n$ reduces to

$$\begin{aligned} 0 = (m+n)\Big(&\cos[\pi\tilde{x}_\pm(4m+2n)/3] - \cos[\pi\tilde{x}_\pm(4n+2m)/3] \\ &- \cos[\pi\tilde{x}_\pm(4m+2n)/3] - \cos[\pi\tilde{x}_\pm(2m-2n)/3] \\ &+ \cos[\pi\tilde{x}_\pm(2n-2m)/3] + \cos[\pi\tilde{x}_\pm(4n+2m)/3]\Big), \end{aligned} \tag{17}$$

which is satisfied for arbitrary $\tilde{x}_\pm$. Similarly, it is easy to show that the terms in Eq. (15) proportional to m and n alone also vanish for arbitrary $\tilde{x}_\pm$. Hence, the TM boundary conditions are precisely satisfied for $\Psi^{o,(1)}_{-m-n,m,n}(x, y)$. A similar procedure confirms that they are also satisfied for $\Psi^{e,(1)}_{-m-n,m,n}(x, y)$. Hence, for each (n, m), the wave function is six-fold degenerate, and is given by Eq. (9). This form for fixed (n, m) can then be used to calculate the radiation patterns obtained by exciting the TM$^z(n, m)$ mode by use of the Love equivalence principle.[19, 20] Calculations of the radiation patterns will be presented elsewhere.

However, it is elementary to demonstrate that the spatial dependencies of the odd and even wave functions are distinct. For example, the ground state contains the odd functions $\Psi^{o,(1)}_{-1,1,0} = -\Psi^{o,(1)}_{-1,0,1}$ and the even functions $\Psi^{o,(1)}_{-1,1,0} = \Psi^{o,(1)}_{-1,0,1}$. These functions have distinctly different nodal curves, as shown in Fig. 4. Note that since $C^{o,(1)}_{1,0} \neq C^{o,(1)}_{0,1}$, the odd function can provide a substantial contribution to the output radiation.

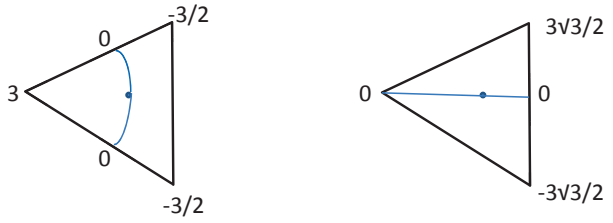

FIG. 4: Left: Values at the corners of $\Psi^{e,(1)}_{-1,0,1}(x,y)$. The nodal curve is also shown. Right: Values at the corners of $\Psi^{o,(1)}_{-1,0,1}(x,y)$. The nodal line contains $\overline{OA}$.

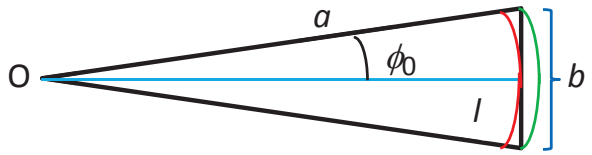

FIG. 5: Sketch of an acute isosceles triangle of long sides a and short side b, with $\ell = \sqrt{a^2 - (b/2)^2}$. The green and red arcs of respective radii a and ℓ when combined with the sides of respective lengths a and ℓ, represent the wedge approximations to the shape of the acute isosceles triangle.

ACUTE ISOSCELES TRIANGLES

To date, no exact solution of the modes and wave functions of a general isosceles triangle has been published. We have studied this problem in detail, and have also concluded that an exact solution of that problem is still elusive. However, for the case of a very acute isosceles triangle, an exact solution to an accurate approximation of the general, highly acute isosceles triangle is possible. The closely related exactly solvable problem is that of a "piece of pie", or a "pie-shaped" wedge. We choose two such wedges to circumscribe the acute isosceles triangle, as sketched in Fig. 5. In this model, $\phi_0 = \tan^{-1}(b/2a)$ and $\ell = \sqrt{a^2 - (b/2)^2}$. The main point is that the exact acute triangle fits between the two circumscribing wedges of radii a and ℓ, respectively. Thus, in the limit $b \to 0$, $a \to \ell$, the two models are equal, and thus represent an exact solution to the problem of an infinitely acute isosceles triangle.

Solution of the wedge cavity with TM boundaries

It is rather elementary to obtain the exact solution of the wave function of a general "pie-shaped" wedge cavity with TM boundary conditions. We first write the wave equation in polar (ρ, ϕ) coordinates,

$$\frac{\partial^2\Psi}{\partial\rho^2} + \frac{1}{\rho}\frac{\partial\Psi}{\partial\rho} + \frac{1}{\rho^2}\frac{\partial^2\Psi}{\partial\phi^2} = -k^2\Psi, \tag{18}$$

where $\Psi(\rho,\phi)$. Using separation of variables, we write

$$\Psi(\rho,\phi) = \sum_\nu R_\nu(\rho)\Phi_\nu(\phi), \tag{19}$$

$$\Phi_\nu(\phi) = A_\nu\cos(\nu\phi) + B_\nu\sin(\nu\phi). \tag{20}$$

Note that both odd and even functions of ϕ are allowed by symmetry. We then obtain the Bessel equation for $R_\nu(\rho)$,

$$\rho^2R''(\rho) + \rho R'(\rho) - \nu^2R(\rho) + k^2\rho^2R(\rho) = 0, \tag{21}$$

where $R' = dR/d\rho$, etc. Letting $x = k\rho$, this reduces to

$$x^2R''(x) + xR'(x) - \nu^2R(x) + x^2R(x) = 0. \tag{22}$$

This has the solution of the Bessel function of the first kind,

$$R_\nu(x) = J_\nu(x) = J_\nu(k\rho). \tag{23}$$

For the TM boundary conditions, the component of the derivative of the wave function normal to the boundaries must vanish. This condition implies

$$\left.\frac{d\Phi_\nu(\phi)}{d\phi}\right|_{\phi=\pm\phi_0} = 0, \tag{24}$$

$$\left.\frac{dR_\nu(\phi)}{d\rho}\right|_{\rho=a,\ell} = 0, \tag{25}$$

where Eq. (24) implies that parity is an important quantity. For solutions with even parity,

$$\Phi^{(e)}_\nu(\theta) = \cos(\nu^{(e)}_n\phi), \tag{26}$$

$$\nu^{(e)}_n = \frac{n\pi}{\phi_0}, \tag{27}$$

for integral n.

Solutions with odd parity have the forms

$$\Phi^{(o)}_\nu(\phi) = \sin(\nu^{(o)}_n(\theta), \tag{28}$$

$$\nu^o_n(\phi) = \frac{(2n+1)\pi}{2\phi_0}, \tag{29}$$

where n is also an integer. From Eq. (25), we then have

$$J'_{\nu^{(o,e)}_n}[k^{(o,e)}_{\max}(m)\ell] = 0, \tag{30}$$

$$J'_{\nu^{(o,e)}_n}[k^{(o,e)}_{\min}(m)a] = 0, \tag{31}$$

for the short (ℓ) and long (a) paths, respectively, where m denotes the m^{th} zero of the first derivative of $J_{\nu^{(o,e)}_n}(x)$, where $J_\nu(x)$ is a Bessel function of the first kind with the non-integral subscript ν that is regular at the origin. We finally obtain that the solutions are given by

$$J'_{\nu^{(o,e)}_n}[\chi(m,\nu^{(o,e)}_n)] = 0, \tag{32}$$

$$f = \frac{c_0\chi(m,\nu^{(o,e)}_n)}{2\pi n_r(\ell,a)}, \tag{33}$$

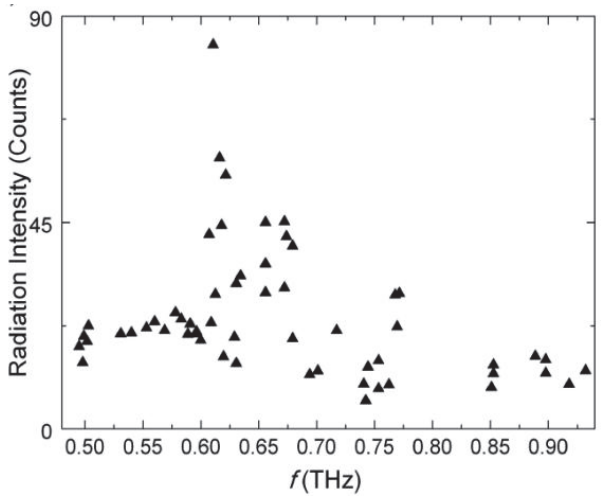

FIG. 6: Intensity versus frequency in THz spectrum measured by a Fourier transform infrared spectrometer from an acute isosceles triangle with $a = 340$ μm, $b = 90$ μm. [21]

m	$\chi(m,\nu_0^{(e)})$	f (THz)	$\chi(m,\nu_0^{(o)})$	f (THz)	$\chi(m,\nu_1^{(e)})$	f (THz)
1	3.8317	0.128	13.7037	0.458	26.0115	0.870
2	7.0156	0.234	18.5548	0.620	31.7446	1.06
3	10.1713	0.340	22.4302	0.750	40.1713	
4	13.3237	0.445	26.0405	0.871	47.6492	
5	16.4706	0.551	29.5184	0.987		
6	19.6159	0.656	32.9167	1.10		
7	22.7601	0.761				
8	25.9037	0.866				
9	32.1897	1.076				

TABLE I: Table of the lowest TM resonance frequencies for a thin isosceles triangular mesa with $a = 340\mu$m and $b = 90\mu$m, for which $\ell = 337\mu$m, $\nu_0^{(e)} = 0$, $\nu_0^{(o)} = 11.8334$ and $\nu_1^{(e)} = 23.6668$.

where (ℓ, a) implies either ℓ or a, corresponding to the two wedge radii. The quantity $\chi(m,\nu_n^{(o,e)})$ represents the m^{th} zero of the first derivative of $J_{\nu_n^{(o,e)}}(x)$, n_r is the index of refraction, which for Bi2212 along the c-axis direction is 4.2,[12] and c_0 is the speed of light in vacuum. The set of lowest $\chi(m,\nu_n^{(o,e)})$ values and the predicted cavity mode frequencies for an acute triangular Bi2212 mesa with $a = 340$ μm and $b = 90$ μm are presented in Table 1.

In Fig. 6, the frequency spectrum of an acute triangular mesa with $a = 340\mu$m and $b = 90\mu$m is shown.[21] We note that the largest peak in the spectrum is for $f \approx 0.62$ THz, which is very close to that predicted for the second odd wave function of our wedge model, as listed in Table 1. Additional peaks are also in close agreement with those predicted for additional odd and even modes. Note that for the shape parameters of the mesa, ℓ and a differ by less than 1%, so this model is highly accurate for such acute isosceles triangles, and is in remarkable agreement with the observed intensity of the radiation.[21] Thus, we anticipate that both types of solutions, odd and even about the line connecting an acute triangular vertex and its center of mass, will be important.

More details and the angular distributions obtained by exciting the various acute isosceles triangular cavity modes will be presented elsewhere.

CONCLUSIONS

We studied the transverse magnetic electromagnetic modes of very thin equilateral and acute isosceles triangular cavities. For equilateral triangular cavities, each cavity frequency is six-fold degenerate, with one-half of the degenerate modes being odd functions about the line passing between the center of gravity and a corner. These new wave-function components could lead to modifications of the angular distribution of the output radiation from those which could have been predicted previously. In addition, we found an exact solution to a wedge model that closely approximates the shape of a highly acute isosceles triangle. The predicted modes are in excellent agreement with experiment.

* Electronic address: klemm@physics.ucf.edu

[1] B. Ferguson and X. C. Zhang, Nat. Mater. **1**, 26 (2002).
[2] M. Tonouchi, Nat. Photonics **1**, 97 (2007).
[3] R. A. Klemm, *Layered Superconductors Volume 1*, (Oxford University Press, Oxford, UK and New York, NY, 2002).
[4] R. Kleiner, F. Steinmeyer, G. Kunkel, and P. Müller, Phys. Rev. Lett. **68**, 2394 (1992).
[5] L. Ozyuzer, A. E. Koshelev, C. Kurter, N. Gopalsami, Q. Li, M. Tachiki, K. Kadowaki, T. Yamamoto, H. Minami, H. Yamaguchi, T. Tachiki, K. E. Gray, W.-K. Kwok, and U. Welp, Science **318**, 1291 (2007).
[6] K. Kadowaki, H. Yamaguchi, K. Kawamata, T. Yamamoto, H. Minami, I. Kakeya, U. Welp, L. Ozyuzer, A. E. Koshelev, C. Kurter, K. E. Gray, and W.-K. Kwok, Physica C **468**, 634 (2008).
[7] H. Minami, I. Kakeya, H. Yamaguchi, T. Yamamoto, and K. Kadowaki, Appl. Phys. Lett. **95**, 232511 (2009).
[8] H. B. Wang, S. Guénon, J. Yuan, A. Iishi, S. Arisawa, T. Hatano, T. Yamashita, D. Koelle, and R. Kleiner, Phys. Rev. Lett. **102**, 017006 (2009).
[9] L. Ozyuzer, Y. Simsek, H. Koseoglu, F. Turkoglu, C. Kurter, U. Welp, A. E. Koshelev, K. E. Gray, W.-K. Kwok, T. Yamamoto, K. Kadowaki, H. B. Wang, and P. Müller, Supercond. Sci. Technol. **22**, 114009 (2009).
[10] H. B. Wang, S. Guénon, B. Gross, J. Yuan, Z. G. Jiang, Y. Y. Zhong, M. Y. Li, A. Iishi, P. H. Wu, T. Hatano, R. G. Mints, E. Goldobin, D. Koelle, H. B. Wang, and R. Kleiner, Phys. Rev. Lett. **105**, 057002 (2010).
[11] S. Guénon, M. Grünzweig, B. Gross, J. Yuan, Z. G. Jiang, Y. Y. Zhong, M. Y. Li, A. Iishi, P. H. Wu, T. Hatano, R.

G. Mints, E. Goldobin, D. Koelle, H. B. Wang, and R. Kleiner, Phys. Rev. B **82**, 214506 (2010).
[12] K. Kadowaki, M. Tsujimoto, K. Yamaki, T. Yamamoto, T. Kashiwagi, H. Minami, M. Tachiki, and R. A. Klemm, J. Phys. Soc. Jpn. **79**, 023703 (2010).
[13] M. Tsujimoto, K. Yamaki, K. Deguchi, T. Yamamoto, T. Kashiwagi, H. Minami, M. Tachiki, K. Kadowaki, and R. A. Klemm. Phys. Rev. Lett. **105**, 037005 (2010).
[14] K. Yamaki, M. Tsujimoto, T. Yamamoto, A. Furukawa, T. Kashiwagi, H. Minami, and K. Kadowaki, Optics Exp. **19**, 3193 (2011).
[15] T. Kashiwagi, K. Yamaki, M. Tsujimoto, K. Deguchi, N. Orita, T. Koike, R. Nakayama, H. Minami, T. Yamamoto, R. A. Klemm, M. Tachiki, and K. Kadowaki, J. Phys. Soc. Jpn. **80**, 094709 (2011).
[16] T. Kashiwagi, M. Tsujimoto, T. Yamamoto, H. Minami, K. Yamaki, K. Delfanazari, K. Deguchi, N. Orita, T. Koike, R. Nakayama, T. Kitamura, M. Sawamura, S. Hagino, K. Ishida, K. Ivanovic, H. Asai, M. Tachiki, R. A. Klemm, and K. Kadowaki, Jap. J. Appl. Phys. **51**, 010113 (2012).
[17] T. M. Benseman, A. E. Koshelev, K. E. Gray, W.-K. Kwok, U. Welp, K. Kadowaki, M. Tachiki, and T. Yamamoto, Phys. Rev. B **84**, 064523 (2011).
[18] M. Tsujimoto, T. Yamamoto, K. Delfanazari, R. Nakayama, T. Kitamura, M. Sawamura, T. Kashiwagi, H. Minami, M. Tachiki, K. Kadowaki, and R. A. Klemm, Phys. Rev. Lett. **108**, 107006 (2012).
[19] R. A. Klemm and K. Kadowaki, J. Phys.: Condens. Matter **22**, 375701 (2010).
[20] R. A. Klemm, E. R. LaBerge, D. R. Morley, T. Kashiwagi, M. Tsujimoto, and K. Kadowaki, J. Phys.: Condens. Matter **23**, 025701 (2011).
[21] K. Delfanazari, H. Asai, M. Tsujimoto, T. Kashiwagi, T. Kitamura, T. Yamamoto, M. Sawamura, K. Ishida, R. A. Klemm, T. Hattori, and K. Kadowaki, submitted to Optics Exp. (unpublished).
[22] J. Helszajn and D. S. James, IEEE Trans. Microwave Theory and Techniques, **MTT-26**, 95 (1978).